
Article:
Kim, Sanghoon, De Bruyn, Mario orcid.org/0000-0002-9687-1606, Louvain, Nicolas et al. (7 more authors) (2019) Green electrode processing using a seaweed-derived mesoporous carbon additive and binder for LiMn2O4 and LiNi1/3Mn1/3Co1/3O2 lithium ion battery electrodes. Sustainable Energy and Fuels. pp. 450-456.

https://doi.org/10.1039/c8se00483h

Sustainable Energy & Fuels

Accepted Manuscript

This article can be cited before page numbers have been issued, to do this please use: S. Kim, M. De bruyn, J. G. Alauzun, N. Louvain, N. Brun, D. J. Macquarrie, L. Stievano, B. Boury, P. H. Mutin and L. Monconduit, *Sustainable Energy Fuels*, 2019, DOI: 10.1039/C8SE00483H.

ROYAL SOCIETY OF CHEMISTRY

rsc.li/sustainable-energy

View Article Online
DOI: 10.1039/C8SE00483H

Journal Name

ARTICLE

Green electrode processing using seaweed-derived mesoporous carbon additive and binder for $LiMn_2O_4$ and $LiNi_{1/3}Mn_{1/3}Co_{1/3}O_2$ lithium ion battery electrodes

Received 00th January 20xx,
Accepted 00th January 20xx

DOI: 10.1039/x0xx00000x

www.rsc.org/

Sanghoon Kim,[a,*] Mario De bruyn,[b] Nicolas Louvain,[a,c] Johan G. Alauzun,[a] Nicolas Brun,[a] Duncan J. Macquarrie,[b] Bruno Boury,[a] Lorenzo Stievano,[a,c] P. Hubert Mutin,[a] and Laure Monconduit,[a,c,*]

Eco-friendly and cheap lithium ion battery electrode processing using seaweed-derived mesoporous carbon additive (Starbon® A800) and binder (sodium alginate) were elaborated for $LiMn_2O_4$ (LMO) and $LiNi_{1/3}Mn_{1/3}Co_{1/3}O_2$ (NMC) lithium ion batteries. Compared to electrodes made using conventional formulations (i.e. Super P/PVDF) the 'green' electrodes can provide significantly 'upgraded' reversible capacity, almost reaching their theoretical capacity at low C-rate, likely due to a good accessibility of lithium ion via mesopores of the carbon additive. In addition, a synergistic effect was observed for a binary carbon additive system composed of Starbon® A800 with a conventional carbon black (Super P), improving both the initial capacity and the rate capability of LMO and NMC electrodes.

Introduction

Renewable materials and processes complying with the principles of green chemistry must be used as much as possible for the elaboration of energy storage devices to make them sustainable. Lithium ion batteries have attracted considerable attention as promising power sources for electronic devices or electric vehicles, due to their high energy density and long cycle life compared to lead–acid, nickel–cadmium, nickel metal hydride batteries.[1,2] Typically, electrodes for lithium ion batteries are obtained from a slurry prepared by mixing an electroactive material with a conductive additive (e.g., carbon black) and a polymeric binder (e.g. polyvinylidene fluoride, PVDF) in an organic solvent (e.g. N-methyl-2-pyrrolidone, NMP), which is tape casted onto an aluminium or a copper current collector. Although the mainstream of the research on lithium ion batteries has been the development of different kinds of cathode and anode materials or their modification by nano-structuration[3,4] or doping,[5,6] the research on improving electrochemically inactive materials such as carbon additives and binders cannot be overlooked because they also participate to the performance of lithium ion batteries.[7-10] With an increase of concern on environmental issues, eco-friendly electrode processing based on water-soluble binders as alternative to fluorine-based conventional binders has emerged.[11-13]

Many studies have shown that polysaccharide-based binders such as carboxymethyl cellulose (CMC) or sodium alginate can improve the cycle life over cycling or the high rate capability of positive ($LiMn_2O_4$,[14] $LiNi_{1/3}Mn_{1/3}Co_{1/3}O_2$,[15] $LiNi_{0.5}Mn_{1.5}O_4$[16], $LiCoPO_4$[17]) and negative electrode materials (Si,[11] $Li_4Ti_5O_{12}$[12]), mainly thanks to their good electrochemical stability, strong adhesion ability and high Young's modulus, which provide a buffer effect for volume change of active materials during cycling.[11] However, most previously reported studies on 'green' electrode processing still used conventional carbon blacks (e.g., Super P, acetylene black), which are generally synthesized by industrial cracking or partial combustion processes. Although these carbon blacks exhibit good electronic conductivity, they are usually non-porous, which might hamper the accessibility of active materials by the lithium ions. Accordingly, these so-called 'green' electrodes do not fully satisfy the main prerequisites of eco-friendly or sustainable chemistry.

The role of conductive carbon additives in lithium ion batteries is principally to provide good electronic conductivity within the electrode over cycling. To improve the characteristic of carbon additives, various methods including surface modification or structuration have been investigated. In particular, a porous structure was found to significantly improve the electrode performance by improving also the ionic conductivity, allowing a faster electrolyte diffusion via porous network.[18-19]

Recently, Starbon® and its derivatives have been developed as sustainable biomass-derived carbonaceous materials with a high mesoporosity.[20-23] The physicochemical properties of Starbon®, including texture, morphology and electronic conductivity can be easily tuned by varying the polysaccharide source (e.g., starch, alginic acid, or pectin), or the parameters of

[a] Institut Charles Gerhardt Montpellier, Université de Montpellier, CNRS, 34090 Montpellier, France. E-mail: sanghoon.kim@umontpellier.fr (SK) laure.monconduit@umontpellier.fr (LM).
[b] Green Chemistry Centre of Excellence, University of York, York, North Yorkshire, YO10 5DD, UK
[c] Réseau sur le Stockage Electrochimique de l'Energie (RS2E), CNRS FR3459, 33 Rue Saint Leu, 80039 Amiens Cedex, France

† Electronic Supplementary Information (ESI) available: See DOI: 10.1039/x0xx00000x

the carbonization process. Starbon® materials have been employed as both catalysts[24,25] and catalyst supports,[26,27] as sorbents for pollutant removal,[28,29] and as porous templates for the synthesis of a mesoporous electrode material.[30] Starbon® materials have also recently been used as alternative carbon additives in negative electrodes ($Li_4Ti_5O_{12}$, TiO_2) of lithium ion batteries, significantly improving the battery performance compared to conventional carbon black additives[31] as Starbon® materials could provide both a good electronic conductivity and an effective lithium ion pathway through its mesoporous structure.

We report here an eco-friendly and cheap 'green' electrode processing using seaweed-derived mesoporous carbon additive (Starbon® A800 from alginic acid) and binder (sodium alginate) for two positive electrode materials: $LiMn_2O_4$ (LMO) and $LiNi_{1/3}Mn_{1/3}Co_{1/3}O_2$ (NMC) (Fig. 1), both already commercialized in the field of electric vehicles (e.g., Nissan LEAF and Chevrolet Bolt). Compared to electrodes made using conventional formulation (i.e., carbon black/PVDF), the 'green' electrodes provide significantly improved reversible capacity reaching their theoretical capacity at low C-rate, mainly thanks to the enhanced diffusion of Li^+ through the mesopores of the carbon additive. In addition, a synergistic effect was observed for electrodes made using a binary carbon additive system (A800:Super P, weight ratio of 6:1) and sodium alginate binder, which significantly improved both initial capacity and rate capability compared to the conventional electrodes. Moreover, the 'green' $LiMn_2O_4$ electrode showed remarkable cycling stability with > 98 % of capacity retention after 100 cycles at 1 C, while less than 95 % of capacity retention observed for a conventional $LiMn_2O_4$ electrode.

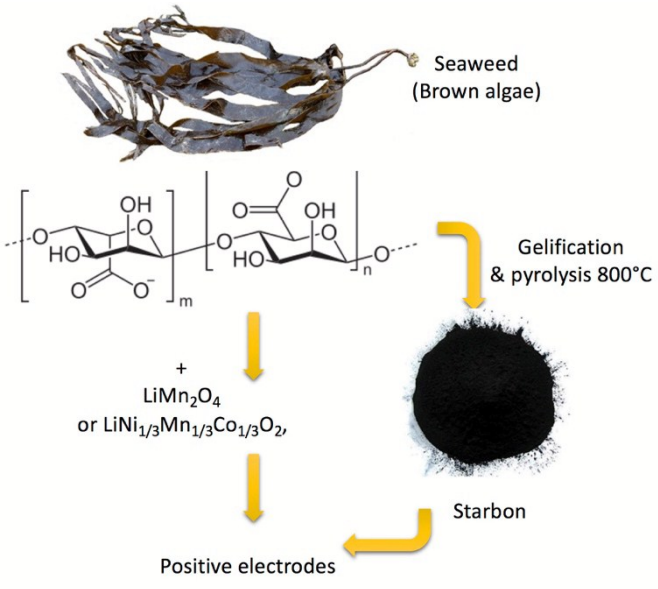

Fig. 1 Schematic representation of 'green' electrode processing using seaweed-derived mesoporous carbon additive and binder for positive electrodes in lithium ion batteries

Experimental

Materials

Alginic acid from brown algae was purchased from Sigma-Aldrich (France). Sodium alginate was purchased from Acros (France). Super P (> 99 %) was purchased from Alfa Aesar (France). Lithium manganese oxide ($LiMn_2O_4$, LMO, BET surface area of 7 m^2 g^{-1}, pore volume of 0.02 cm^3 g^{-1}, Fig. S1a for SEM image) and lithium nickel manganese cobalt oxide ($LiNi_{1/3}Mn_{1/3}Co_{1/3}O_2$, NMC, BET surface area of less than 1.0 m^2 g^{-1}, pore volume of less than 0.02 cm^3 g^{-1}, Fig. S1b for SEM image) were purchased from Targray (Canada). All reagents were used without further purification.

Synthesis of seaweed (alginic acid)-derived mesoporous carbon A800.

First, an alginic acid solution (4.8 wt% in water) was gelled by heating at 90 °C for 2.5 h, and then kept at 4 °C for 24 h. Afterwards, *tert*-butyl alcohol (TBA) was added to the gel, to reach the eutectic composition (30 wt% TBA, 70 wt% water). The mixture was stirred for 1h at RT and then kept for 24 h without stirring and finally freeze-dried (-55°C). The so-obtained dried expanded gel of alginic acid was then pyrolyzed at 800 °C for 3 h (argon flow: 50 mL min^{-1}, heating rate: 1 °C min^{-1}) giving the mesoporous carbon material A800 (A stands for alginic acid, 800 for the carbonization temperature in °C) with a yield of ca. 25 wt%.

Characterization

N_2 physisorption experiments were carried out at -196 °C on a Micromeritics 3Flex; all materials were degassed at 120°C for 15 h at $5{\cdot}10^{-2}$ mbar before the physisorption measurements. Scanning electron microscopy (SEM) images were acquired with a Hitachi S-4800 electron microscope. EDX analyses were acquired with a JEOL CENTURIO detector. The electronic conductivity of carbon additives was measured by 4-point probe method on pellets (30 mg carbon + 2 mg polytetrafluoroethylene PTFE, 13 mm diameter) prepared with a FT-IR pellet press (5 tons).

Galvanostatic electrochemical characterizations were performed at room temperature on a BTS3000 instrument from Neware Battery. Electrochemical impedance spectroscopy (EIS) studies were done on a BioLogic VSP instrument, from 100 kHz to 20 mHz, with a 10 mV amplitude in potentiostatic mode at the end of the discharge (3.4 V). Electrodes are composed of the active material (80 wt%), carbon additive (10 wt%), and sodium alginate (10 wt%), except if mentioned otherwise. In the case of Super P/PVDF electrodes, the slurries are composed of the active material (80 wt%), Super P (10 wt%), and polyvinylidene fluoride (Solef 5130, 10 wt%) and N-methyl-2-pyrrolidone (NMP, Sigma-Aldrich) was used as solvent, instead of water. After stirring in water or NMP, the slurry was mixed using an agate grinding jar (1 h at 500 rpm), then tape casted uniformly at 150 µm onto an aluminum current collector (0.018 mm, 99.0 %, Goodfellow) using a 3540 bird film applicator (Elcometer). Electrodes (diameter 12.7 mm) were then cut out with a disk cutter and dried under vacuum at 120 °C for 15 h. The loading weight per electrode disk was approximatively

2.5 mg. CR2032 coin-type cells were assembled in a glove box under Ar atmosphere (O_2 < 0.5 ppm, H_2O < 0.5 ppm), using lithium metal as both reference and counter electrode. The electrolyte was LP30 (0.2 mL, 1M $LiPF_6$ dissolved in a mixture of ethylene carbonate (EC) and dimethyl carbonate (DMC) (ratio EC : DMC = 1:1). Whatman glass fibre disks were used as separators. The electrochemical galvanostatic measurements were taken in the voltage range of 3.4-4.3 V vs Li^+/Li for LMO, 2.8V-4.4 V vs Li^+/Li for NMC, respectively.

Results and discussion

Characterization of seaweed (alginic acid)-derived mesoporous carbon Starbon® A800

The seaweed-derived mesoporous carbon (Starbon® A800) used in this study as a carbon additive was prepared from a dried mesoporous expanded gel of alginic acid, which was prepared by gelatinization, solvent removal and then pyrolysis at 800 °C as previously reported.[31,32] The textural properties of A800 are summarized in Table 1, along with those of a commercial carbon additive, Super P (see Fig. S2 for N_2 physisorption isotherm). The electronic conductivity of A800 (84 S m^{-1}, three times lower than that of Super P) is moderate, mainly due to the low degree of graphitization and low C:O atomic ratio. However, this value is significantly higher than for other commercial mesoporous carbons, especially starch-derived Starbon® S800 (24 S m^{-1}) or resorcinol-formaldehyde gel-based NC® carbon series (32 S m^{-1}),[31] probably due to the fibrous aggregation of carbonized alginic acid linear chains (Fig. 3 for SEM images), which might provide an effective electron conduction pathway.

Table 1. Textural properties, electronic conductivity and C:O ratio of carbon additives

Carbon additive	S_{BET} (m^2 g^{-1})	PV_{total} (cm^3 g^{-1})	PV_{meso} (cm^3 g^{-1})	D_p (nm)	σ (S m^{-1})	C:O atomic ratio
A800	490	0.91	0.71	16.0	84	16.9
Super P	50	0.13	0.09	-	279	> 100

S_{BET}: BET specific area determined by BET method; PV_{total}: total pore volume at P/P_0 = 0.99; PV_{meso}: BJH mesopore volume between 2 and 50 nm; D_p: BJH average mesopore diameter (desorption branch); σ: electronic conductivity; C:O atomic ratio obtain by SEM-EDX.

The XRD pattern of A800 (Fig. 2a) shows two broad peaks at 22.5° and 44.0°, which could be ascribed to the (002) and (100) reflections of graphite (JCPDS 75-1621), demonstrating a turbostratic-like carbon structure.[21] The Raman spectrum of A800 (Fig 2b) presents two distinct broad peaks at 1360 cm^{-1} (D-band) and 1590 cm^{-1} (G-band). The intensity ratio of I_D/I_G is 0.81, indicating a pseudo-graphitic structure with a low degree of ordering. Super P appears slightly more graphitized with more intense peaks for (002) and (100) reflection in XRD patterns and a lower I_D/I_G ratio.

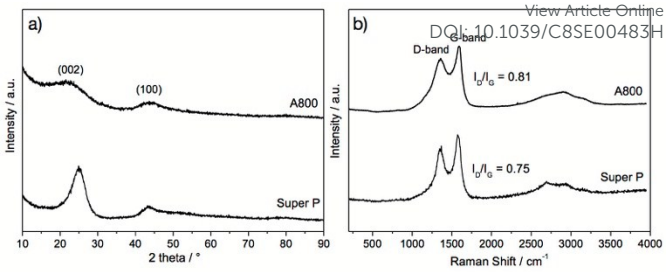

Fig. 2. a) Powder X-ray diffraction patterns of carbon additives b) Raman spectra of carbon additives. The ratio I_D/I_G calculated based on the intensity of D-band (1360 cm^{-1}) and G-band (1590 cm^{-1}).

SEM images analysis indicated that A800 is composed of fibrous aggregates (Fig. 3a), which arise from the rearrangement of alginic acid chains, and also of foam-like aggregates (indicated by white arrows in Fig. 3c). The mesopores are clearly seen at high magnification (Fig. 3b) and their size (ca. 20 nm) is consistent with the pore size obtained by N_2 physisorption experiment (Table. 1). The SEM image of Super P (Fig. 3d) shows randomly aggregated spherical nanoparticles, about 50 nm in size, accounting for the specific surface area.

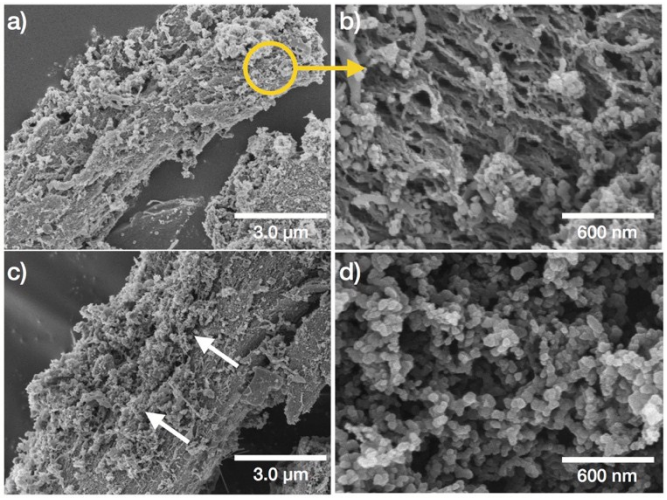

Fig. 3. SEM images of a), b) and c) A800 and d) Super P.

Electrochemical performance of $LiMn_2O_4$, $LiNi_{1/3}Mn_{1/3}Co_{1/3}O_2$ 'green' electrodes made using A800 and sodium alginate

The electrochemical performance of $LiMn_2O_4$ and $LiNi_{1/3}Mn_{1/3}Co_{1/3}O_2$ 'green' electrodes made using A800 as carbon additive and sodium alginate as binder was evaluated in CR2032 coin-type half-cells using lithium metal as counter and reference electrode.

Fig. 4a and 4b show the galvanostatic charge/discharge profiles of LMO electrodes made using A800/alginate, and Super P/PVDF at 0.1 C, respectively. The specific discharge capacity of the LMO/A800/alginate electrode was 147 mAh g^{-1} at 5th cycle, which is very close to the theoretical capacity of LMO (148 mAh g^{-1}), while the LMO/Super P/PVDF electrode showed only 96 mAh g^{-1} as 5th discharge capacity. The first-cycle coulombic efficiency was 88 % and 69 % for LMO/A800/alginate and LMO/Super P/PVDF electrodes, respectively. Indeed, it is

generally known that better coulombic efficiency for the first cycle can be obtained for electrodes made using water processable binders such as CMC or alginate.[11] In the case of NMC (Fig. 4c and 4d), the specific discharge capacity of NMC/A800/alginate electrode is 182 mAh g^{-1} at 5th cycle, approximately 50 mAh g^{-1} higher than that of NMC/Super P/PVDF electrode. This gain of capacity for both LMO and NMC 'green' electrodes can be ascribed to the good accessibility of the surface of the active material by the lithium ions via the mesopores of A800. This finding is very interesting because LMO or NMC electrodes made using bulk type active materials (i.e. non-porous without nano-structuration) often showed very low specific capacity,[33-36] generally due to the non-porous structure of the active material, the lack of electrochemical activity or the poor accessibility the material by lithium ions. However, these results show that the poor performance of bulk materials can be simply overcome by generating mesoporosity within the electrode using a mesoporous carbon additive such as A800. Besides, the contribution of A800 to the capacity is negligible, as a blank electrode formulated with only A800 and carbon black showed a capacity only ca. 20 mAh g^{-1}, corresponding to ~2 mAh g^{-1} for LMO or NMC electrodes. (Fig. S3)

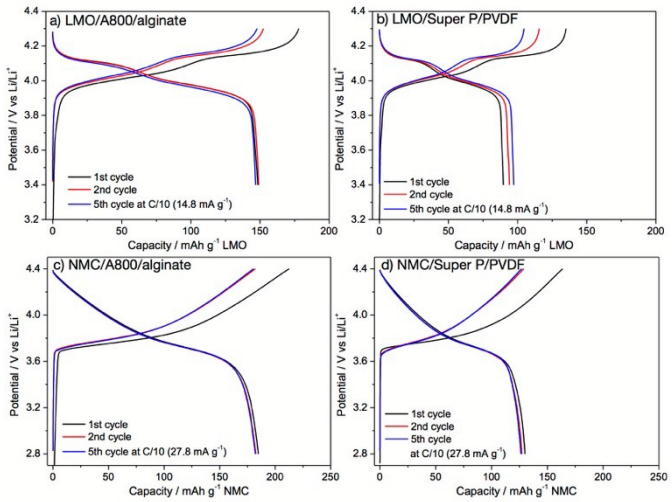

Fig. 4 Galvanostatic charge–discharge curves for a) LMO/A800/alginate, b) LMO/Super P/PVDF, c) NMC/A800/alginate and d) NMC/Super P/PVDF electrodes cycled at C/10 (14.8 mA g^{-1} for LMO, 27.8 mA g^{-1} for NMC)

When higher applied current densities (Fig. 5a and 5b), both LMO and NMC electrodes formulated with A800 and alginate showed a rapid capacity drop, especially in the case of LMO electrode, which displayed a specific capacity of only 21 mAh g^{-1} at 1C. The capacity decrease for the NMC/A800/alginate electrode is less important than that for the LMO/A800/alginate one, even though its capacity at 6C and 8C is still poorer than that of NMC/Super P/PVDF electrode. The capacity drop at high rate is not related to the sodium alginate binder, as LMO and NMC electrodes formulated using Super P/alginate showed similar results to those made using Super P/PVDF, except for the improved first-cycle coulombic efficiency (87 %). Thus, the poor rate capability can be more likely ascribed to the moderate electronic conductivity of A800. From these results, it could be suggested that at low current densities the electrochemical performance is dominated by lithium ion transfer, which in our case can be facilitated by the mesopores, while the electronic conductivity becomes more a limiting factor at higher current densities. Indeed, this has been recently proved by our group, where a mesoporous LMO with or without carbonaceous species grafted on the surface was prepared to discriminate the respective roles of mesoporosity and conductivity.[30] In addition to the porosity and the conductivity of the additives, the intrinsic conductivity of the active materials during charge/discharge could explain the difference of the capacity drop between LMO and NMC at high current densities. Indeed, LMO and NMC have a low conductivity of 10^{-5} and 10^{-7} S cm^{-1} in the discharged (lithiated) state, respectively. Then, their conductivity changes deeply upon charge (delithiation) giving 10^{-4} S cm^{-1} for LMO and 10^{-2} S cm^{-1} for NMC. In other words, NMC rapidly becomes very conductive with an increase by five orders of magnitude of its conductivity, while that of LMO remains of the same order of magnitude.[37,38]

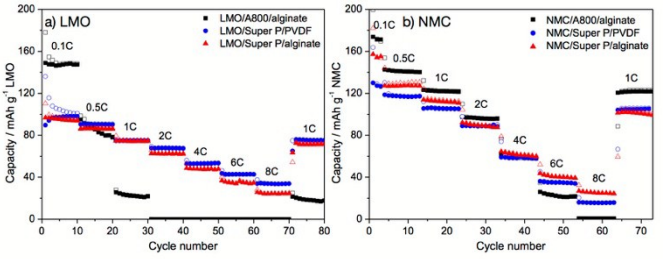

Fig. 5. Rate capability of a) LMO and b) NMC electrodes made using different carbon additives and binders.

To improve the rate capability of LMO/A800/alginate electrodes, we investigated the performance of electrodes formulated with sodium alginate and a binary carbon (BC) additive, composed of a mixture of A800 and Super P with different A800:Super P weight ratios (from 1:3 to 6:1 for BC13 to BC61). As shown in Fig. 6a, even a small amount of Super P in the mixture (A800:Super P ratio = 6:1) drastically improved the performance of the LMO electrode compared to LMO/A800/alginate electrodes (Fig. 5a), with an increase of the specific discharge capacity from 95 mAh g^{-1} to 131 mAh g^{-1} at 0.1 C. The specific capacity at high 6C or 8C rates was less sensitive to the composition of the binary carbon additive, but remained in all cases slightly higher than that of the LMO/Super P/PVDF electrode. This result demonstrates again that both the conductivity and the porosity of carbon additives have a strong impact on the performance of the electrodes and that a synergistic effect can be obtained by balancing the contribution of both types of carbon. In addition, the improvement of electrochemical performance for LMO/BC61/alginate could also explained by an improved electrode stability during cycling. SEM images of LMO/Super P/PVDF electrode after cycling (Fig. S4) show that Super P particles seems to be separated from LMO particles, which might result in a lack of contact, and that some macroporosity formed upon cycling. On the contrary, after cycling LMO/BC61/alginate electrodes still show a

View Article Online
DOI: 10.1039/C8SE00483H

compact morphology without any crack and the carbon particles appear homogeneously dispersed (Fig. 1d).

The influence of the amount of the binary carbon additive (A800:Super P ratio fixed to 6:1, labelled BC61) on the electrochemical performance was also investigated (Fig. 6b). From 4 to 13 wt% of BC61, the specific capacity and rate capability of the LMO electrode increased rapidly with the amount of additive, reaching an optimum for 13 wt%. For higher BC61 additive contents, 16 and 20 wt%, the specific discharge capacity decreased, however an acceptable retention of capacity was found even at high rate.

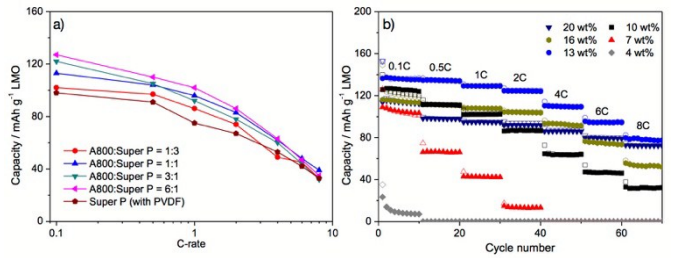

Fig. 6. a) Rate capability of LMO electrode formulated with different ratio of binary carbon additive system; b) Influence of the amount of the binary carbon additive (BC61) on the rate capability of LMO electrodes.

The BC61 system provided an excellent long term cyclability for LMO electrode with a discharge capacity of 121 mAh g^{-1} after 100 cycles at 1C, corresponding to > 98 % of capacity retention (Fig. S5a), and a coulombic efficiency after 100 cycles of 99.1 %. By comparison, LMO/Super P/PVDF electrode showed a capacity retention of only 94 % under the same conditions with a coulombic efficiency of 98.7 % after 50 cycles, while the cell became unstable after 100 cycles. (Fig. S5b)

The enhanced electrochemical performance of LMO electrode made using BC61 additive and sodium alginate can be further evidenced by electrochemical impedance spectroscopy (EIS). As shown in Fig. 7, the Nyquist plots for both electrodes exhibited a depressed single semicircle in the middle to high frequency range, which could reflect both the charge transfer resistance (R_{ct}) between electrolyte and LMO surface and cathode electrolyte interfacial resistance (CEI, R_{sf}) formed at the surface of the LMO particles. An oblique line at the low-frequency region can be interpreted as Warburg impedance, which is characteristic of bulk lithium diffusion.[39-41] Upon cycling, this semicircle slightly decreased for both electrodes, finally becoming stable after 5 cycles. By fitting using an equivalent model (Fig. S6, Table S1) on 10th cycle, the charge transfer resistance (R_{ct}) and cathode electrolyte interfacial resistance (R_{sf}) were calculated to be 20 Ω and 87 Ω for LMO/BC61/alginate electrode, and 32 Ω and 178 Ω for LMO/Super P/PVDF electrode, respectively. Interestingly, the resistance after 5 cycles for the alginate based electrode is even smaller than that of 1st cycle or fresh cell, which is not the case for the PVDF-based electrode. Thus, it can be suggested that the CEI layer of both electrodes is stable, but that the CEI layer of LMO/BC61/alginate is less resistive than that of LMO/Super P/PVDF. However, both electrodes show similar Warburg diffusion coefficient (σ) with the same magnitude order as the same LMO material was used.

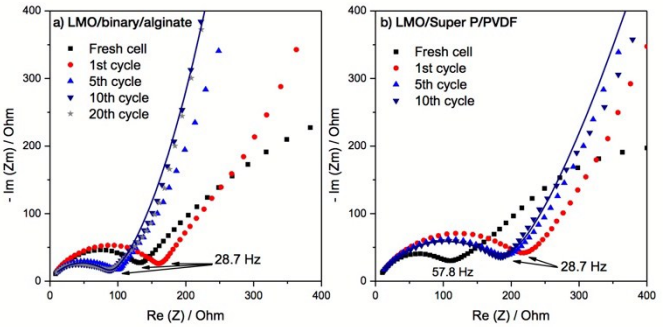

Fig. 7. Nyquist plots of a) LMO/binary carbon/alginate electrode and b) LMO/Super P/PVDF electrode during cycling at C/10. Fitting was performed on 10th cycle.

The performance of the 'green' LMO electrode prepared using BC61 and sodium alginate additives is also compared to LMO electrodes performance reported in the literature (Table 2) Despite the non-porous texture of the LMO active material in this study, our 'green' LMO electrode provides a high specific capacity and a good rate capability and compares well with previously reported works (Table 2). However, it should be noted that many parameters as the electrode thickness, the active material loading, the cell fabrication can vary from a reference to another, making direct comparison difficult.

Table 2. Comparison of the performance of selected LMO electrodes

Active material	Electrode composition (wt%)[a]	Specific capacity (mAh g^{-1})	Rate capability (mAh g^{-1})	Ref
Bulk type LMO	AM/BC61/alginate (77/13/10)	138 mAh g^{-1} at 0.1 C	85 mAh g^{-1} at 8 C	This work
Bulk type LMO	AM/hollow carbon/PVDF (80/10/10)	125 mAh g^{-1} at 0.1 C	45 mAh g^{-1} at 4 C	18
Porous LMO	AM/CB/PVDF (70/20/10)	105 mAh g^{-1} at 0.1 C	92 mAh g^{-1} at 10 C	42
Mesoporous LMO	AM/CB/PVDF (80/10/10)	138 mAh g^{-1} at 0.2 C	70 mAh g^{-1} at 4 C	33
C, N coated bulk type LMO	AM/CB/PVDF (80/10/10)	130 mAh g^{-1} at 0.2 C	90 mAh g^{-1} at 5 C	43
V_2O_5 coated LMO nanoparticles	AM/CB/PVDF (70/20/10)	122 mAh g^{-1} at 0.2 C	108 mAh g^{-1} at 2 C	44[b]
Bi, La doped LMO nanoparticles	AM/CB/PVDF (80/10/10)	123 mAh g^{-1} at 1 C	95 mAh g^{-1} at 7 C	45[c]
LMO/CNT composite	AM/CNT (90/10)	128 mAh g^{-1} at 0.2 C	50 mAh g^{-1} at 5 C	46[d]

[a] AM refers to active material, CB to carbon black such as Super P or acetylene black. [b] electrode loading of 3-6 mg. [c] electrode thickness of 0.1 mm. [d] electrode loading of 2 mg cm^{-2}. The current density corresponding to 1 C for $LiMn_2O_4$ is 148 mA g^{-1}.

Finally, our approach of designing binary composition of carbon additives (BC61) was also applied to NMC electrodes, which showed promising results both at low and high rates (Fig. 8); capacities of 170 mAh g^{-1} at 0.1 C and 42 mAh g^{-1} at 8 C were obtained when only 129 mAh g^{-1} at 0.1C and 16 mAh g^{-1} at 8 C were measured for the conventional NMC electrode (i.e., SuperP/PVDF). However, the gain in electrochemical performance is less important compared to LMO electrodes, mainly due to the higher intrinsic conductivity of NMC during charge/discharge, as discussed above.

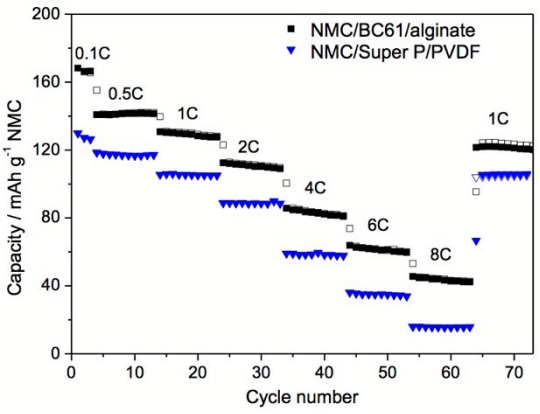

Fig. 8. Rate capability of NMC electrode formulated with BC61 (A800:Super P=6:1)/alginate or with Super P/PVDF.

Conclusion

In summary, we have shown that an eco-friendly and cheap lithium ion battery electrode processing using seaweed derived mesoporous carbon additive (Starbon® A800) and binder (sodium alginate) allows improving the reversible capacity of LMO and NMC electrodes at low C-rate, mainly thanks to a facilitated Li^+ diffusion via the mesoporous structure of A800. A binary carbon additive (A800:Super P, weight ratio of 6:1, BC61) combined with sodium alginate significantly improves both the initial capacity and the rate capability compared to conventional Super P/PVDF electrodes. Based on these results, it can be proposed that at low C-rate, the electrochemical performance of LMO and NMC electrodes is strongly dependent on their accessibility by lithium ions, which can be facilitated by the mesoporous structure of A800, while the electronic conductivity (provided by Super P) becomes more important at high C-rate. In a similar way, tuning the contributions of porosity and electronic conductivity by mixing different types of carbon additives could be a simple and effective way to optimise the electrochemical performance of other electrode materials too.

Conflicts of interest

There are no conflicts to declare.

Acknowledgements

Financial support was received from the European Commission in the framework of POROUS4APP project (H2020 GA no. 666157). The authors would like to thank Didier Cot (IEM, France) for SEM analysis.

References

1 M. Armand and J. M. Tarascon, *Nature*, 2008, **451**, 652–657.
2 G. E. Blomgren, *J. Electrochem. Soc.*, 2016, **164**, A5019–A5025.
3 A. S. Aricò, P. Bruce, B. Scrosati and J. M. Tarascon, *Nature Materials*, 2005.
4 J. Jiang, Y. Li, J. Liu, X. Huang, C. Yuan and X. W. D. Lou, *Adv. Mater.*, 2012, **24**, 5166–5180.
5 F. Kong, R. C. Longo, D.-H. Yeon, J. Yoon, J.-H. Park, C. Liang, S. KC, Y. Zheng, S.-G. Doo and K. Cho, *J. Phys. Chem. C*, 2015, **119**, 21904–21912.
6 L. Liu, H. Zhang, J. Yang, Y. Mu and Y. Wang, *Chem. Eur. J.*, 2015, **21**, 19104–19111.
7 M. E. Spahr, D. Goers, A. Leone, S. Stallone and E. Grivei, *J. Power Sources*, 2011, **196**, 3404–3413.
8 J. Zheng, J. Xiao, W. Xu, X. Chen, M. Gu, X. Li and J.-G. Zhang, *J. Power Sources*, 2013, **227**, 211–217.
9 H. Zheng, R. Yang, G. Liu, X. Song and V. S. Battaglia, *J. Phys. Chem. C*, 2012, **116**, 4875–4882.
10 S. Komaba, N. Yabuuchi, T. Ozeki, Z.-J. Han, K. Shimomura, H. Yui, Y. Katayama and T. Miura, *J. Phys. Chem. C*, 2011, **116**, 1380–1389.

11 I. Kovalenko, B. Zdyrko, A. Magasinski, B. Hertzberg, Z. Milicev, R. Burtovyy, I. Luzinov and G. Yushin, *Science*, 2011, **334**, 75–79.
12 B.-R. Lee and E.-S. Oh, *J. Phys. Chem. C*, 2013, **117**, 4404–4409.
13 A. Magasinski, B. Zdyrko, I. Kovalenko, B. Hertzberg, R. Burtovyy, C. F. Huebner, T. F. Fuller, I. Luzinov and G. Yushin, *ACS Appl. Mater. Interfaces*, 2010, **2**, 3004–3010.
14 M.-H. Ryou, S. Hong, M. Winter, H. Lee and J. W. Choi, *J. Mater. Chem. A*, 2013, **1**, 15224–6.
15 N. Loeffler, J. von Zamory, N. Laszczynski, I. Doberdo, G.-T. Kim and S. Passerini, *J. Power Sources*, 2014, **248**, 915–922.
16 F. Bigoni, F. De Giorgio, F. Soavi and C. Arbizzani, *J. Electrochem. Soc.*, 2016, **164**, A6171–A6177.
17 E. J. Kim, X. Yue, J. T. S. Irvine and A. R. Armstrong, *J. Power Sources*, 2018, **403**, 11-19.
18 J. Wutthiprom, N. Phattharasupakun and M. Sawangphruk, *ACS Omega*, 2017, **2**, 3730–3738.
19 Q. Zhang, G. Peng, G. Wang, M. Qu and Z. L. Yu, *Solid State Ionics*, 2009, **180**, 698–702.
20 V. Budarin, J. H. Clark, J. J. E. Hardy, R. Luque, K. Milkowski, S. J. Tavener and A. J. Wilson, *Angew. Chem. Int. Ed.*, 2006, **45**, 3782–3786.
21 R. J. White, C. Antonio, V. L. Budarin, E. Bergström, J. Thomas-Oates and J. H. Clark, *Adv. Funct. Mater.*, 2010, **20**, 1834–1841.
22 R. J. White, V. L. Budarin and J. H. Clark, *Chem. Eur. J.*, 2010, **16**, 1326–1335.
23 R. J. White, V. Budarin, R. Luque, J. H. Clark and D. J. Macquarrie, *Chem. Soc. Rev.*, 2009, **38**, 3401–18.
24 R. Luque, V. Budarin, J. H. Clark and D. J. Macquarrie, *Appl Catal B*, 2008, **82**, 157–162.
25 R. Luque, V. Budarin, J. H. Clark and D. J. Macquarrie, *Green Chemistry*, 2009, **11**, 459–3.
26 R. Luque, J. H. Clark, K. Yoshida and P. L. Gai, *Chem. Commun.*, 2009, 5305–3.
27 J. C. Colmenares, P. Lisowski and D. Łomot, *RSC Adv.*, 2013, **3**, 20186–7.
28 H. L. Parker, A. J. Hunt, V. L. Budarin, P. S. Shuttleworth, K. L. Miller and J. H. Clark, *RSC Adv.*, 2012, **2**, 8992–6.
29 A. Muñoz García, A. J. Hunt, V. L. Budarin, H. L. Parker, P. S. Shuttleworth, G. J. Ellis and J. H. Clark, *Green Chemistry*, 2015, **17**, 2146–2149.
30 S. Kim, M. De bruyn, J. G. Alauzun, N. Louvain, N. Brun, D. Macquarrie, L. Stievano, B. Boury, L. Monconduit and P. H. Mutin, *J. Mater. Chem. A*, 2018, **6**, 14392-14399.
31 S. Kim, A. M. Escamilla-Pérez, M. De bruyn, J. G. Alauzun, N. Louvain, N. Brun, D. Macquarrie, L. Stievano, B. Boury, L. Monconduit and P. H. Mutin, *J. Mater. Chem. A*, 2017, **5**, 24380–24387.
32 A. Borisova, M. De Bruyn, V. L. Budarin, P. S. Shuttleworth, J. R. Dodson, M. L. Segatto and J. H. Clark, *Macromol. Rapid Commun.*, 2015, **36**, 774–779.
33 S. Chen, Z. Chen and C. Cao, *Electrochim. Acta*, 2016, **199**, 51–58.
34 W. Sun, H. Liu, T. Peng, Y. Liu, G. Bai, Sen Kong, S. Guo, M. Li and X.-Z. Zhao, *J. Mater. Chem. A*, 2015, **3**, 8165–8170.
35 K. M. Shaju and P. G. Bruce, *Adv. Mater.*, 2006, **18**, 2330–2334.
36 Z. Chen, J. Wang, D. Chao, T. Baikie, L. Bai, S. Chen, Y. Zhao, T. C. Sum, J. Lin and Z. Shen, *Sci. Rep.*, 2016, 1–10.
37 M. Nishizawa, T. Ise, H. Koshika, T. Itoh and I. Uchida, *Chem. Mater.*, 2000, **12**, 1367–1371.
38 R. Amin and Y.-M. Chiang, *J. Electrochem. Soc.*, 2016, **163**, A1512–A1517.
39 X. Li, K. Zhang, S. Wang, M. Wang, F. Jiang, Y. Liu, Y. Huang and J. Zheng, *Sustainable Energy Fuels*, **2018**, 2, 1772–1780.
40 X. Li, K. Zhang, D. Mitlin, Z. Yang, M. Wang, Y. Tang, F. Jiang, Y. Du and J. Zheng, *Chem. Mater*. **2018**, 30, 2566−2573.
41 X. Li, K. Zhang, D. Mitlin, E. Paek, M. Wang, F. Jiang, Y. Huang, Z. Yang, Y. Gong, L. Gu, W. Zhao, Y. Du and J. Zheng, *Small*, **2018**, 1802570.
42 L. J. Xi, H.-E. Wang, Z. G. Lu, S. L. Yang, R. G. Ma, J. Q. Deng and C. Y. Chung, *J. Power Sources*, 2012, **198**, 251–257.
43 P. R. Ilango, K. Prasanna, S. J. Do, Y. N. Jo and C. W. Lee, *Sci. Rep.*, 2016, **6**, 29826.
44 H. Ming, Y. Yan, J. Ming, J. Adkins, X. Li, Q. Zhou and J. Zheng, *Electrochim. Acta*, 2014, **120**, 390–397.
45 C.-G. Han, C. Zhu, G. Saito and T. Akiyama, *RSC Adv.*, 2015, **5**, 73315–73322.
46 X. Jia, C. Yan, Z. Chen, R. Wang, Q. Zhang, L. Guo, F. Wei and Y. Lu, *Chem. Commun.*, 2011, **47**, 9669–3.

View Article Online
DOI: 10.1039/C8SE00483H

145x129mm (300 x 300 DPI)